

RESEARCH

Open Access



Macrophage-derived SPP1 exacerbate myocardial injury by interacting with fibroblasts in viral myocarditis

Xiuyun Duan^{1†}, Li Zhang^{2,3,5†}, Keyu Liu^{1,5}, Kaiyin Guo⁶, Yingnan You^{2,3,5}, Hailin Jia^{2,3,5}, Shan Zhou^{2,3,5} and Bo Han^{1,2,3,4,5*} 

Abstract

Background Viral myocarditis (VMC) is an inflammatory myocardial condition triggered by viral infections which involves pathogenic-related damage and immune-mediated damage. However, the precise immunopathogenic mechanisms underlying VMC remain elusive.

Methods We performed single-cell RNA sequencing on mouse hearts during the acute phase of CVB3-induced VMC. After manually annotating cell types, functional analyses of macrophage were performed by cell ratio changes, customized gene set module scoring and CellPhoneDB. Utilizing indirect co-culture experiments in vitro, the effects of macrophage-derived SPP1 on cardiac fibroblasts were investigated. Depletion of macrophages and inhibition of SPP1 expression in mice were carried out to study the effects of macrophage-derived SPP1 on cardiac function, inflammation levels, and myocardial injury in mice with VMC.

Results Our data revealed that macrophages are the major immune cells which infiltrate the heart during the acute phase of VMC, particularly a macrophage subpopulation which highly expresses *Spp1* (*Spp1*⁺ macrophages) and exhibited characteristics of peripheral blood monocytes. *Spp1*⁺ macrophages communicate extensively with fibroblasts during VMC, and that SPP1 promotes fibroblast conversion to an inflammatory phenotype with high *Ccl2*/*Ccl7* expression. This in turn increases monocyte chemotaxis to the heart. Besides, a partial depletion of macrophages in the early stages of VMC attenuated myocardial inflammation and myocardial injury in mice. Inhibition of SPP1 reduced cardiac macrophage infiltration, attenuated myocardial inflammation, and improved cardiac function in VMC mice.

Conclusion Our findings suggested that *Spp1*⁺ macrophages could self-recruit, and macrophage-derived SPP1 exacerbated myocardial immune injury by promoting high *Ccl2*/*Ccl7* expression in fibroblasts. Our study advances understandings of VMC pathogenesis, and provides novel insight into potential immunotherapies for VMC.

Keywords Viral myocarditis, Single-cell analysis, Macrophages, Fibroblasts, SPP1

[†]Xiuyun Duan and Li Zhang contributed equally to this work.

*Correspondence:

Bo Han

hanbo35@163.com; 198657000056@email.sdu.edu.cn

Full list of author information is available at the end of the article



Introduction

Myocarditis is a common disease, particularly in children and adolescents [1]. However, due to insufficient understandings of the underlying etiologies and pathogenesis of myocarditis, there is currently a lack of specific and effective treatments for the conditions. Roughly 30% of patients with myocarditis may develop dilated cardiomyopathy, which has a five-year survival rate of less than 50% [2]. Thus, elucidating complex disease mechanisms and devising effective therapies is crucial.

Myocarditis refers to inflammatory myocardial lesions related to non-ischemic etiologies [3]. Infectious conditions are important drivers of myocarditis, with enteroviruses, particularly Coxsackie virus B (CVB), being the most common causative pathogens. The pathogenesis of viral myocarditis (VMC) is currently believed to involve direct damage caused by pathogen infections and indirect damage caused by secondary immune responses. During the acute phase of myocarditis, an influx of immune cells infiltrates myocardial tissue, and interact with cardiomyocytes, fibroblasts, endothelial cells and other cardiac cells. However, the specific roles of cardiac cells, infiltrating immune cells, gene expression profiles, and cellular communication in myocarditis are still not fully understood.

Jiangping Song et al. studied the single-cell transcriptional profiles of cardiac immune cells collected during different experimental autoimmune myocarditis (EAM) phase, and detailed the immunological network underlying EAM for the first time [4]. Han Zhu et al. reported peripheral immune profiles of patients with immune checkpoint inhibitor (ICI) myocarditis, and found an expansion of specialized effector CD8⁺T cells (Temra CD8⁺ cells) in the peripheral blood [5]. Daowen Wang et al. studied the single-cell transcriptional landscapes and cell-cell communications of cardiomyocytes, infiltrating immune cells, and peripheral immune cells in mice with fulminant myocarditis [6]. However, the transcriptional profiles of non-cardiomyocyte cells, including cardiac fibroblasts, endothelial cells, and mural cells, as well as any of their communications with immune cells, have not yet been studied.

In 2020, a study published in *Nature* reported on the full repertoire of adult cardiac cells, and showed that cardiac fibroblasts were the most abundant type of cells in cardiac tissue after cardiomyocytes, accounting for 20–25% of all atrial and ventricular cells [7]. The classic function of cardiac fibroblasts is extracellular matrix synthesis and degradation, which helps maintain tissue homeostasis. Prior to this, most studies on myocarditis had been focused on cardiomyocytes, and often neglected the role of fibroblasts. One study pointed out that, in the pathogenesis of inflammatory dilated cardiomyopathy, cardiac fibroblasts secreted key chemokines

and cytokines which shaped immune cell chemotaxis and differentiation [8]. However, there are still insufficient understandings of the proportional and phenotypic changes in cardiac fibroblasts during the acute phases of myocarditis.

Here, we established a single-cell landscape of immune cells and cardiac cells during the acute phase of VMC, which provides comprehensive insight into immune responses and cell-cell communications. We predominantly focused on macrophages and fibroblasts, both of which showed significant proportional and transcriptional changes during the acute disease phase. Our findings suggest that *Spp1*⁺ macrophages both self-recruit and exacerbate myocardial immune injuries by promoting high *Ccl2/Ccl7* expression in fibroblasts. This study contributes to increased understandings of the mechanisms underlying inflammation in VMC, and may help lead to novel treatment targets for the condition.

Materials and methods

Mice

4-5-week-old male BALB/c mice were purchased from Beijing Vital River Laboratory Animal Technology Co., Ltd. Viral myocarditis mouse model was constructed by intraperitoneal injection of 200 μ L 10⁶ TCID50 Coxsackie virus B3 (CVB3, strain Nancy). Bacteria-free phosphate buffer solution (PBS) was used as a control. General conditions and weight were recorded daily until sacrifice on day7. This study was approved by the Animal Ethical Committee of Shandong Provincial Hospital Affiliated to Shandong First Medical University. All procedures complied with the Guide for the Care and Use of Laboratory Animals, published by the National Institutes of Health.

Macrophage depletion

For the macrophage depletion, mice were intravenously injected with 200 μ L Clophosome[®]-Clodronate Liposomes (FormuMax Scientific, USA) the day before CVB3 injection, and supplemental doses of 150 μ L were injected every 3 days. PBS was used as a control.

SPP1 inhibition

For the SPP1 inhibition, mice were intravenously injected with 250 μ g osteopontin (also called Secreted Phosphoprotein 1, SPP1) expression inhibitor (MedChemExpress, China) the day before CVB3 injection and supplementally injected every 3 days. The solvent of SPP1 expression inhibitor was used as a control.

Human plasma samples

Plasma samples of 7 health controls and 12 myocarditis patients were collected from patients hospitalized in Shandong Provincial Hospital with written informed consent. Sample collection was performed according to

the Declaration of Helsinki. Myocarditis was diagnosed according to 2013 Position Statement of the European Society [3], and the 2021 American Heart Association scientific statement on the diagnosis and treatment of childhood myocarditis [1]. The demographics and clinical features of patients is listed in Supplementary Table 1.

Cell isolation and culture

Bone marrow-derived macrophages (BMDMs) were obtained from 4-5-week-old male BALB/c mice. Briefly, bone marrow cells were rinsed from the femur and tibia of the mice and cultured in RPMI-1640 medium (Gibco, USA) supplemented with 10% fetal bovine serum (ExCell Bio, China) and 1% penicillin-streptomycin (BasalMedia, China) for 24 h. Then cells were seeded into 6-well plates at a density of 6×10^5 cells/well and differentiated with 20 ng/ml M-CSF (Biolegend, USA). The medium was replaced every other day. After 6 days of differentiation, the BMDMs were stimulated by 100 μ L 10^6 TCID₅₀ CVB3 per well for 12 h and the control group had no special treatment. Mouse cardiac fibroblasts cell lines were purchased from Shanghai Zhong Qiao Xin Zhou Biotechnology Co., Ltd. and were cultured in special medium with fibroblast growth factor (PCM-M-186, ZQXZBIO, China). The murine cardiac muscle cell line HL-1 was purchased from Shanghai Zhong Qiao Xin Zhou Biotechnology Co., Ltd. and cultured in Minimum Essential Medium (Gibco, USA) with 10% fetal bovine serum and 1% penicillin-streptomycin. All cells were cultured at 37 °C with 5% CO₂.

Co-culture of BMDMs and fibroblasts

In order to minimize viral effects, differentiated BMDMs were washed well with PBS after 12 h of CVB3 stimulation. The general complete medium was added to continue the incubation for 12 h. Meanwhile, the BMDMs of SEI + CVB3 group were supplemented with 25 μ g of SPP1 expression inhibitor (SEI) dissolved in dimethyl sulfoxide (DMSO) per well. The control group and CVB3 group were supplemented with an equal amount of DMSO solvent. The supernatants were collected and used as BMDM conditioned medium. Cardiac fibroblasts were cultured with special medium mixed with the BMDM conditioned medium at a ratio of 1:1 for 24 h and collected for further experiments.

Histology and pathology

Mouse hearts were paraffin-embedded after being fixed in 4% paraformaldehyde for 24 h at 4 °C. The tissues were cut into 4 μ m thick serial sections. The heart sections were dewaxed and hydrated, and then subjected to hematoxylin-eosin (HE) and Masson's trichrome staining by standard protocols. Myocarditis scoring criteria are as follows: 0 indicates no inflammation; 1 indicates 1–5

distinct mononuclear inflammatory foci with $\leq 5\%$ cross-sectional area involvement; 2 indicates more than 5 distinct mononuclear inflammatory foci or $>5\%$ but $\leq 20\%$ cross-sectional area involvement; 3 indicates diffuse mononuclear inflammation with $>20\%$ area involvement without necrosis; 4 indicates diffuse inflammation with necrosis and acute inflammation [9].

Immunofluorescence

Paraffin tissue Sect. (4 μ m thick) were dewaxed, hydrated, antigen repaired, permeabilized and blocked. Next, the slides were incubated overnight at 4 °C with primary antibodies including anti-CD68 rabbit antibody (1:200, GB113109, Servicebio, China) or anti-SPP1 goat antibody (5 μ g/ml, AF808, R&D, USA). After PBS washing, the slides were then incubated with Alexa Fluor® 488-conjugated Goat Anti-Rabbit IgG (1:200, GB25303, Servicebio) or Cy3 conjugated Donkey Anti-Goat IgG (1:300, GB21404, Servicebio) for 1 h at room temperature under light-proof conditions. DAPI was used to stain the cell nuclei. Fluorescence images were visualized under EVOS M7000 3D digital confocal analysis system (Invitrogen, USA).

TUNEL staining

Cardiac tissue apoptosis was assessed using the TUNEL BrightRed Apoptosis Detection Kit (A113, Vazyme, China) following the manufacturer's instructions. The apoptotic nuclei were stained with red fluorescence, and cell nuclei were counterstained with DAPI. Pictures were obtained by a researcher who was blind to this study using the EVOS M7000 microscope (Invitrogen, USA).

Flow cytometry

Mouse spleens were isolated and prepared into single cell suspensions. Macrophages were identified using FITC anti-mouse F4/80 Antibody (123109, BioLegend, USA) and APC anti-mouse CD45 Antibody (110713, BioLegend, USA). Apoptosis rates of HL-1 cells were measured using the BD Pharmingen™ PE Annexin V Apoptosis Detection Kit I, following the manufacturer's protocol.

Cell counting Kit-8 assay

The Cell Counting Kit-8 (CCK-8) assay was used to assess the cytotoxicity of SPP1 on HL-1 cells. When the cell density reached 50%, HL-1 cells were stimulated with different concentrations of SPP1 recombinant protein. After 24 h, Enhanced CCK-8 (E-CK-A362, Elabscience, China) was used to detect cell activity, and absorbance was measured at 450 nm.

Echocardiography

Echocardiography was performed using the Silicon-Wave 60 system with a 30 MHz high frequency probe

(Kolo Medical, China). Mice were anesthetized by isoflurane and maintained normal body temperature by a heated platform. Parasternal long axis 2-dimensional and M-mode images were used to obtain ejection fraction (EF) and fractional shortening (FS).

Real-time quantitative PCR

Total RNA was extracted from tissues or cells using Trizol (Vazyme, China). Quantitative RNA was transcribed into complementary DNA using the HiScript III RT SuperMix for qPCR kit (Vazyme, China). Real-time quantitative PCR (RT-qPCR) reactions were carried out on a Lightcycler 480 system (Roche, Switzerland) using ChamQ Blue Universal SYBR qPCR Master Mix (Vazyme, China). Relative gene expression level was calculated by CT value. Primer sequences are listed in Supplementary Table 2.

Western blot

Tissues or cells were fully lysed on ice for 20 min using RIPA lysis buffer containing protease inhibitors. The lysates were centrifuged at 12,000 g for 20 min at 4 °C and the proteins in the supernatants were taken. Proteins were added to SDS-PAGE for separation followed by transfer to PVDF membranes. The membranes were blocked with 5% nonfat milk in TBST for 1 h at room temperature and incubated overnight at 4 °C with anti-SPP1 (1:1000, sc-73631, Santa Cruz, USA). The second day, membranes were further incubated with HRP-conjugated Affinipure Goat Anti-Mouse IgG (1:5000, SA00001-1, Proteintech, China) for 1 h at room temperature. The protein bands were then visualized using Immobilon Western HRP Substrate (WBKLS0100, Millipore, USA). Next, the membranes were immersed in stripping buffer for 30 min to wash away bound antibodies and re-blocked with nonfat milk. Membranes were incubated with anti- β -actin (1:5000, sc-47778, Santa Cruz, USA) at 4 °C overnight and visualized directly. Western blot results were quantitatively analyzed by imagej software (National Institutes of Health, USA).

Enzyme-linked immunosorbent assay

The plasma and cell supernatant levels of inflammatory factors, SPP1, B-type natriuretic peptide (BNP) and cardiac troponin T (cTnT) were measured using a standard enzyme-linked immunosorbent assay (ELISA) kits following the manufacturer's instructions. All applied ELISA kits are listed in Supplementary Table 3.

Tissue dissociation and single-cell suspension preparation

Cardiac tissue samples were sectioned into 0.5 mm² fragments and chilled on ice, followed by rinsing with calcium- and magnesium-depleted 1×PBS. These samples were then enzymatically processed at 37 °C with

a solution comprising 0.35% Collagenase IV, 2 mg/mL papain, and 120 units/mL DNase, under agitation at 100 rpm for 20 min. The enzymatic reaction was quenched with 1×PBS supplemented with 10% fetal bovine serum, and the mixture was gently pipetted 5–10 times to ensure cell dissociation. The cell mixture was strained and centrifuged at 300 g for 5 min at 4 °C. The pellet was resuspended in 100 μ l of 1×PBS containing 0.04% BSA, treated with erythrocyte lysate (Solarbio, China) for 2–10 min on ice, and centrifuged again at 300 g for 5 min at room temperature. The suspension was then resuspended in 1×PBS with 0.04% BSA and centrifuged twice at 300 g for 3 min at 4 °C. The final cell pellet was resuspended in 50 μ l of 1×PBS with 0.04% BSA, and cell viability, assessed by Trypan blue staining, was confirmed to exceed 85%. The cell concentration was standardized to a range of 700–1200 cells/ μ l.

Single-cell RNA sequencing and data processing

Single-cell suspensions were loaded to 10x Chromium and sequenced on an Illumina NovaSeq 6000 sequencing system by LC-Bio Technology co. ltd (HangZhou, China) at a minimum depth of 20,000 reads per cell. Raw sequencing data were demultiplexed into FASTQ format using Illumina bcl2fastq software, version 2.20. The single-cell RNA sequencing (scRNA-seq) data were aligned to Ensembl genome GRCh38/GRCm38 reference genome. A total of 76,524 cells were captured from three healthy and four diseased samples. Dimensional reduction, clustering, and analysis of scRNA-seq data were carried out. A stringent quality control filter was applied, retaining 68,634 cells with criteria including gene expression per cell between 250 and infinity, UMI counts below infinity, mitochondrial gene content below 25%, and the exclusion of multicellular events using DoubletFinder. These cells underwent dimensionality reduction and were visualized in a 2D UMAP space using Uniform Manifold Approximation and Projection (UMAP). Gene expression values were normalized using the LogNormalize method in Seurat's "Normalization" function, followed by PCA, with the top 20 principal components selected for clustering and UMAP analysis. Cluster identification was facilitated by weighted shared nearest neighbor (SNN) graph clustering, and marker genes were determined based on expression in over 10% of cells within a cluster and an average log₂ Fold Change (log₂FC) of at least 0.26.

Differential expression and functional enrichment analysis

Differential expression analysis was performed using the FindMarkers function of the Seurat package with the "bimod" test. $p < 0.01$, $|\log_2FC| \geq 0.26$ and expression in more than 10% of cells were used to define differentially expressed genes (DEGs). Kyoto Encyclopedia of Genes and Genomes (KEGG) and Gene Ontology (GO)

pathway analysis were performed using the “clusterProfiler” package (version 4.0).

Cell subset annotations and cellular interaction

For cell subset annotations, the Harmony algorithm was used to integrate cells from different samples into a shared space for unsupervised clustering, and the resulting batch-effect correction matrix was used for further analysis. We performed data cleaning on macrophages to remove other cells mixed in with them. Finally, 5 clusters of macrophages (resolution=0.1) and 9 clusters of fibroblasts (resolution=0.4) were identified. CellPhoneDB was used to infer cell–cell interactions.

RNA velocity analysis

RNA rate analysis was used to infer the differentiation trajectory of monocyte macrophages. RNA rates were calculated for each cell using the default settings of the “scvelo” Python package. The velocity field and pseudo-time values were then projected onto a UMAP plot.

Module score calculation

Module scoring was performed based on the AddModuleScore function in the Seurat package [10]. All genes used to calculate gene scores are listed in the Supplementary Table 4.

Statistical analysis

Statistical analysis was performed using GraphPad Prism 9 (GraphPad Software Inc., USA). Differences between the two groups was tested using unpaired Student’s t test and statistical deference among multiple groups were performed using one-way analysis of variance (ANOVA). * $P < 0.05$, ** $P < 0.01$, and *** $P < 0.001$ were considered statistically significant.

Results

Day 7 of CVB3 infection is the peak of inflammation in a VMC mouse model

To elucidate the immunological mechanisms underlying VMC, we first constructed a preliminary CVB3 infected BALB/c mouse model. Mice injected with CVB3 showed increased lethargy, poor appetites, and diarrhea. Two mice died on days 6 and 7. The myocarditis group showed sharp decreases in body weight. These changes gradually recovered after the acute phase (1 week) but still did not reach healthy levels in 21 days after disease onset (Fig. 1A). By measuring LVEF and FS using echocardiography, we found that mouse cardiac function began to decompensate 4 days after CVB3 infection. Without therapeutic measures, this change persisted into day 21 (Fig. 1B, C). Interestingly, pathology showed no significant inflammatory cardiac infiltration on day 4 within our model, and mice had the highest myocarditis

scores on day 7 (Fig. 1D, E, F). These findings suggested that deterioration of cardiac function occurred before the onset of peak inflammation. On day 7 after CVB3 infection, inflammatory plaques had formed on the surface of the heart, and a high degree of inflammatory infiltration could be seen on microscopic examination (Fig. 1D, F). As the disease progressed, fibrosis developed in some mouse hearts (visualized with Masoon staining; Fig. 1G).

We also examined the plasma levels of inflammatory cytokines and myocardial injury markers during disease progression. As expected, on day 7, the levels of IL-1 β , IL-6, IFN- γ , and cTnT were significantly elevated. The secretion of TNF- α also increased, although not statistically significant. There were slight elevations in BNP, this change was not statistically significant, which may be because of marked inter-individual differences in BNP levels (Fig. 1H, I). IL-4 and IL-10 levels did not increase in the early myocarditis stages, but did increase after day 14 (Fig. 1J). Both IL-4 and IL-10 are protective cytokines in VMC [11–13], suggesting that the disease enters a recovery phase after day 14. In summary, our model suggested that day 7 of CVB3 infection was the inflammatory peak in myocarditis. However, the immune cell subtypes that contributed to this inflammatory peak, as well as the transcription changes, remained unclear.

Macrophages are the main immune cells infiltrating the heart in the acute phase of VMC

To investigate the roles of infiltrating immune cells and cardiac cells during the acute phases of VMC, we collected cardiac tissue from three control mice and four CVB3-infected mice during the acute disease phase (day 7), and performed single-cell RNA sequencing (scRNA-seq) using the 10x Genomics Chromium platform. After quality control, a total of 68,634 cells were used for further analysis. Unbiased cluster analysis showed 27 clusters of cardiac cells (Fig. 2A). Manual annotation was performed using the typical markers. We identified seven immune cell types, including macrophages, monocytes, T cells, neutrophils, B cells, natural killer (NK) cells, and dendritic (DC) cells, and five non-immune cell types, including fibroblasts, endothelial cells, mural cells, cardiomyocytes, and glial cells. We also identified proliferative cells and other cell types (Fig. 2B, C and Figure S1A). Fibroblasts were the most predominant non-immune cell type, but decreased in proportion during the acute phase of myocarditis, while endothelial cell populations increased. In cardiac tissue of VMC mice, the macrophage populations expanded more than ten-fold to become the predominant immune cell type (Fig. 2D and Figure S1B~D). Immunofluorescence confirmed this finding (Fig. 2E). GO enrichment pathway analysis of differentially-expressed macrophage genes between the VMC and healthy control groups showed significant

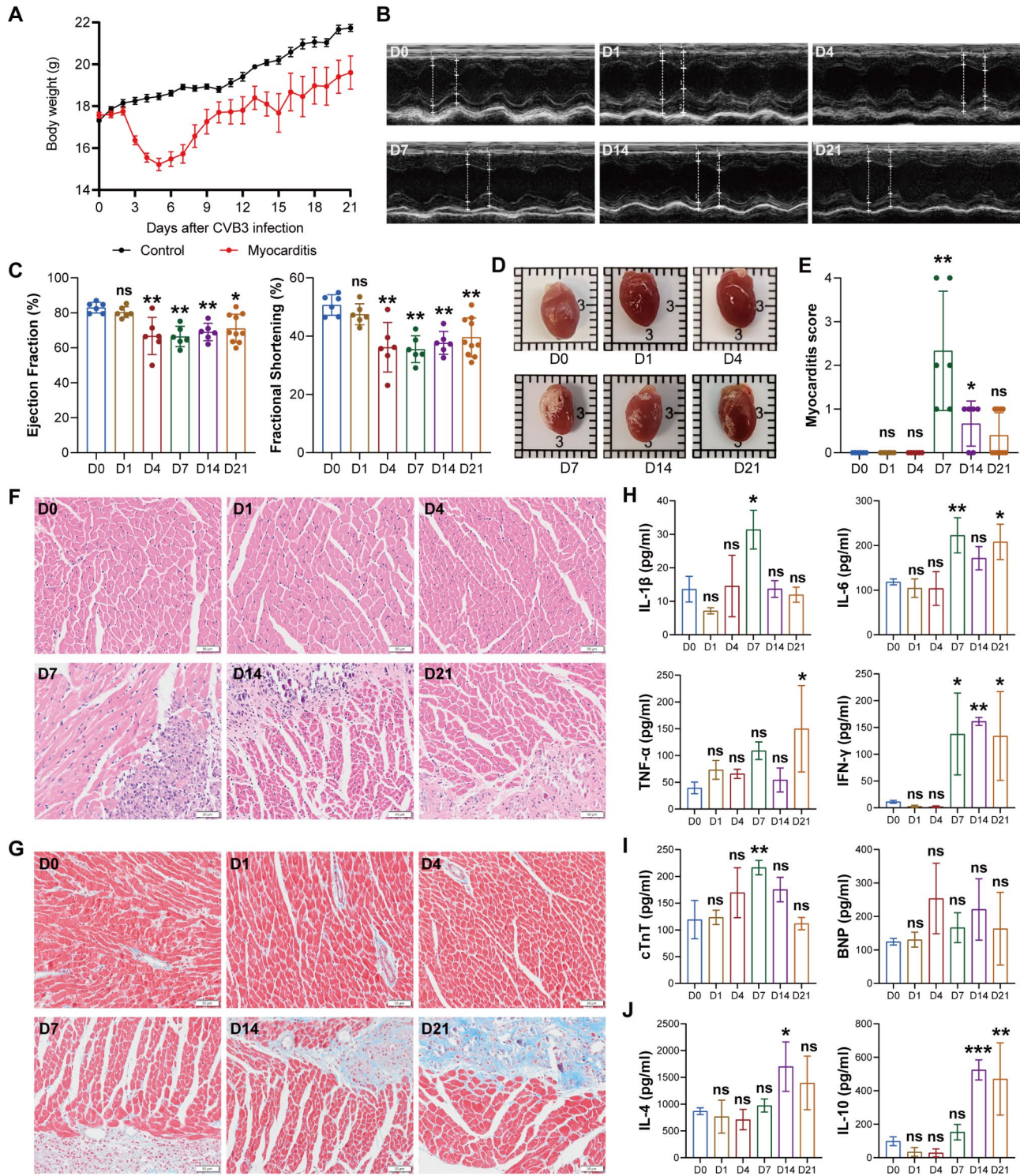


Fig. 1 Disease progression of VMC mice. **(A)** Weight changes of VMC mice during disease progression. **(B)** Representative M-mode echocardiography images of VMC mice at different time points. **(C)** EF and FS of VMC mice at different time points. **(D)** Representative heart images of VMC mice. Heart shrinks and forms geographic-like inflammatory plaque on the surface on day 7. Scale bars: 1 mm. **(E)** Myocarditis scores for immune infiltration at different time points as described in Methods. **(F)** Cardiac immune infiltration status at different time points. Scale bars: 50 μ m. Blue represents fibrosis. Scale bars: 50 μ m. **(H)** The levels of proinflammatory cytokines in the plasma of VMC mice at different time points. **(I)** The expression levels of cTnT and BNP in the plasma of VMC mice at different time points. **(J)** The levels of protective cytokines in the plasma of VMC mice at different time points. Unpaired t-test was used for analysis. Data are presented as mean \pm SD ($n \geq 6$ biologically independent samples). *** $P < 0.001$, ** $P < 0.01$, * $P < 0.05$, ns $P > 0.05$

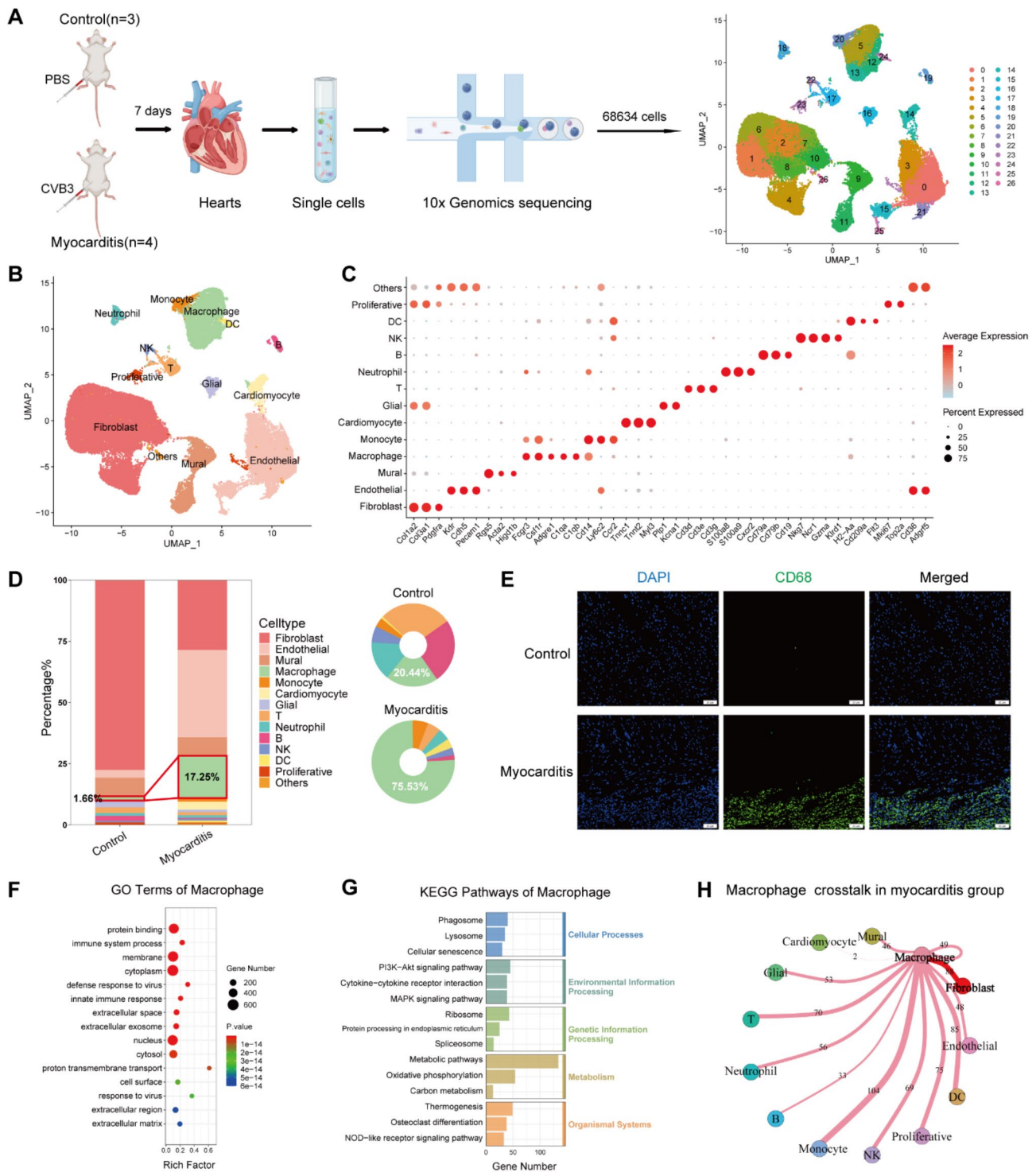


Fig. 2 Single-cell atlas of cardiac cells and infiltrating immune cells in VMC heart, and functional analysis of macrophages. **(A)** Schematic diagram showing scRNA-seq pipeline of cardiac tissues. **(B)** UMAP plot of cardiac cells and infiltrating immune cells colored by cell type. **(C)** Bubble plot of marker genes of each cell type. The dot color represents the gene expression level, and the dot size represents the percentage of cells expressing the respective gene. **(D)** Histogram of all cell population proportions (left) and doughnut chart of immune cell population proportions (right). **(E)** Representative immunofluorescent staining of macrophages (CD68, green) and nuclei (DAPI, blue) in cardiac tissues from control and VMC mice. Scale bars: 50 μ m. **(F)** Top 15 upregulated GO analysis terms of differentially expressed genes (DEGs) between control and VMC mice in macrophages. DEGs used in the analysis were selected with $P < 0.01$ and $|\log_2FC| \geq 0.26$. **(G)** KEGG analysis of DEGs between control and VMC mice in macrophages. **(H)** Interaction strength of ligand-receptor pairs between macrophages and other cell populations in the myocarditis group

changes in several immune response-related pathways (Fig. 2F). KEGG pathway analysis suggested that these differentially-expressed genes (DEGs) were enriched in enhanced cytokine-cytokine receptor interactions, as well as in the activation of PI3K-AKT and MAPK signaling pathways (Fig. 2G). Macrophage phagocytosis and metabolic capacity were also both enhanced in hearts with myocarditis. These data highlight the important role of macrophages in the development of VMC.

We also assessed cell-cell communications between macrophages and other cell types by analyzing interaction weights. We found that macrophages had the strongest interactions with monocytes, followed by fibroblasts (Fig. 2H). Previous studies have shown that fibroblasts promote the conversion of monocytes to macrophages in VMC [14, 15]. We found that both the macrophage clusters and fibroblast clusters changed considerably in acute VMC (Fig. 2D). We conducted further analysis of these two cell clusters.

***Spp1*⁺ macrophages expand in the hearts of VMC mice**

Macrophages are a highly heterogeneous cellular population, and different macrophages perform distinct or even opposing functions in cardiovascular disease [16]. To further identify the subtypes of immune cells that influence the development of VMC, we re-clustered macrophages and identified four clusters. Based on each cluster's characteristic gene expression, the four clusters were sequentially named: *Spp1*⁺ macrophages (highest relative expression of *Spp1* and *Gpnmb*), *C1q*⁺ macrophages (highest expression of complement component 1q), Mito⁺ macrophages (highest expression of mitochondria-associated genes *mt-Rnr1*, *Lars2*, and *mt-Rnr2*), and proliferating macrophages (highest relative expression of proliferation-associated genes *Mcm5*, *Mcm6* and *Mki67*) (Fig. 3A, B and Figure S2A, B). Comparative analysis of cellular proportions revealed that *Spp1*⁺ macrophages were significantly expanded in VMC mice (Fig. 3C, D and Figure S2C). We also analyzed DEGs in overall macrophage populations between the control group and myocarditis group, and similarly found significant increases of *Spp1* in the myocarditis group (Fig. 3E), which was also confirmed by RT-qPCR of cardiac tissues (Fig. 3F). SPP1, which is also known as osteopontin, is involved in a variety of biological processes, including biological mineralization, inflammation, and wound healing [17]. We examined SPP1 protein levels using ELISA and western blots, and found increased SPP1 expression in both plasma and cardiac tissue of VMC mice (Fig. 3G, H). Immunofluorescence tests showed that *Spp1*⁺ macrophage levels increased in the cardiac tissue of VMC mice, which were identified by colocalization of SPP1 and CD68 (Fig. 3I). To determine differentiation and developmental relationships among macrophage subgroups and

monocytes, we performed RNA velocity analysis. Our dynamic velocity analysis model indicated that *Spp1*⁺ macrophages were predominantly derived from monocytes (Fig. 3G), suggesting that expanded *Spp1*⁺ macrophages in the heart benefitted from the recruitment and transformation of peripheral blood monocytes. *C1q*⁺ macrophages, in contrast, might arise from the proliferation and transformation of resident cardiac macrophages. We found that *C1q*⁺ macrophages expressed classical markers of tissue-resident macrophages, such as *Cd163*, *Lyve1* and *Cbr2* [5], while *Spp1*⁺ macrophages showed high levels of *Ccr2*, which is a marker of monocyte-derived macrophages (Fig. 3K). Both *Spp1*⁺ and *C1q*⁺ macrophages eventually differentiated into Mito⁺ macrophages. Among the four major macrophages clusters, *Spp1*⁺ macrophages had the highest proliferation scores and acute inflammation scores (Fig. 3L), although they also exhibited transcriptomic features of M2-type macrophages (Figure S2D). These data suggest that *Spp1*⁺ macrophages may represent an activated cellular population with strong proliferative and inflammatory response capacity in VMC. Collectively, these findings suggest that *Spp1*⁺ macrophages play a major role in the development of VMC.

Macrophage-derived SPP1 drive *Ccl2*⁺*Ccl7*⁺ inflammatory fibroblasts activation

The above single-cell sequencing results revealed that fibroblasts were an abundant cardiac cellular type, and had rich, complex interactions with macrophages in VMC mice (Fig. 2D, H). Differential expression analysis revealed increased *Ccl2* and *Ccl7* expression in fibroblasts in the myocarditis group, although the number and percentage of fibroblasts were reduced (Fig. 4A). This piqued our interest because the transcription proteins of *Ccl2* and *Ccl7* are chemokines that bind to CCR2 receptors, which mediate monocyte mobilization and recruitment from the bone marrow to the site of inflammation [18, 19]. The major histocompatibility complex (MHC)-1 components of fibroblasts, including H2-K1 and H2-D1, were also upregulated in the myocarditis group. GO enrichment analysis revealed that DEGs in fibroblasts between control and myocarditis mice were related to immune responses in VMC (Fig. 4B). This finding is consistent with previous studies, which have shown that fibroblasts can secrete chemokines and inflammatory factors participating in the inflammatory response process during the acute phases of VMC [20].

We next performed unbiased cluster analysis of fibroblasts, and obtained nine clusters (Figure S3A). Five fibroblast populations were identified according to the biological functions of their marker genes (Fig. 4C, D and Figure S3B, C). Inflammatory fibroblasts were enriched in *Cxcl1*, *Ccl2* and *Ccl7*, and were increased in number in

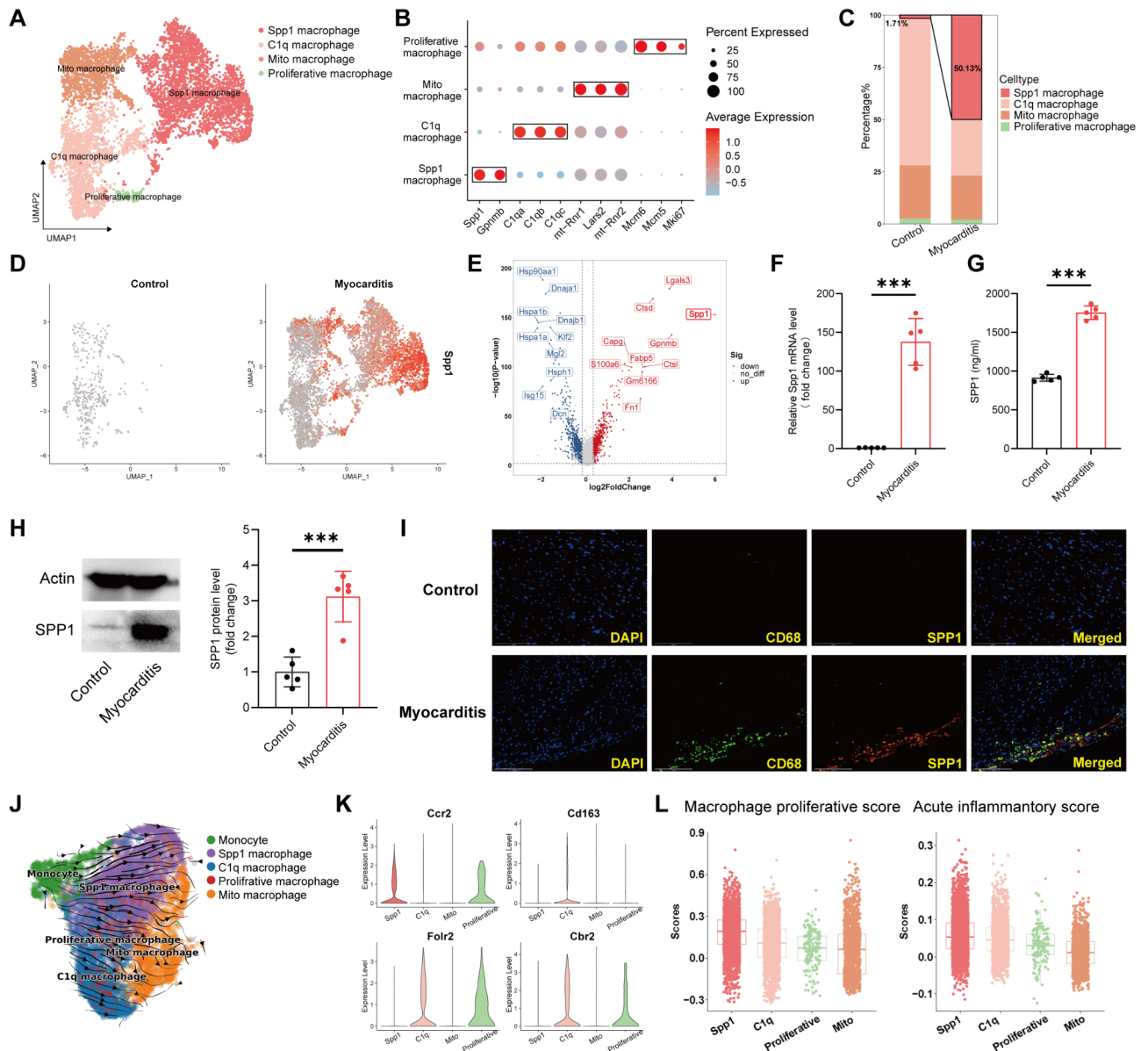


Fig. 3 Expansion of *Spp1*⁺ macrophages in VMC mice. **(A)** UMAP plots of macrophage subpopulations colored by cell type. **(B)** Bubble plot showing the expression levels of cell-typing genes in macrophage subpopulations. **(C)** Histogram of macrophage subpopulations proportions. **(D)** UMAP plots of *Spp1* expression in macrophages from control and VMC mice. The dot color represents the *Spp1* expression level in each cell. **(E)** Volcano plot showing DEGs between control and VMC mice in macrophages. **(F)** Relative *Spp1* mRNA levels in mouse cardiac tissues. **(G)** The expression levels of *SPP1* in mouse plasma. **(H)** Western blotting analysis of SPP1 in mouse cardiac tissues. **(I)** Representative immunofluorescent staining of macrophages (CD68, green), nuclei (DAPI, blue) and SPP1 (red) in cardiac tissues from control and VMC mice. Scale bars: 125 μm . **(J)** UMAP plot showing the dynamical model of macrophages' developmental transition as revealed by RNA velocity. **(K)** Violin plot showing the expression levels of classical markers of tissue-resident macrophages (*Cd163*, *Fcrl2* and *Cbr2*) and *Ccr2* in each macrophage subpopulation. **(L)** Box plot of characteristic scores among different macrophage subpopulations. Unpaired t-test was used for analysis. *** $P < 0.001$, ** $P < 0.01$, * $P < 0.05$, ns $P > 0.05$

the VMC group (Fig. 4E, F and Figure S3D). Matrix fibroblasts abundantly expressed extracellular matrix-related genes (*Mfap5*, *Col4a1*, *Col4a2*, *Cd248*). Cluster 3 was characterized by significant upregulation in WNT signaling pathway inhibitors *Wif1* and *Dkk3*, which we named "Wnt related fibroblasts". This population may originate in the epicardium [21]. Cluster 4 shared many gene expression profiles with cluster 3, and was characterized

by the expression of *Lfgfbp3*, *Fgl2* and *ApoE*. Richard P. Harvey. et al. suggested this cluster may represent an intermediate population between Cluster 3 and another population of fibroblasts [22], which, here, we categorize them to Wnt related fibroblasts. The other two subpopulations were mito fibroblasts (*mt-Rnr2*, *mt-Rnr1*, *Lars2*) and lipid-related fibroblasts (*Vcan*, *Neat1*, *Fabp4*). To understand the cellular communications between

intracellular SPP1 protein levels were elevated (Fig. 5A, B). We next designed an indirect co-culture experiment to verify the effects of SPP1 on cardiac fibroblast expression of *Ccl2* and *Ccl7* (Fig. 5C). We used SPP1 expression inhibitor (SEI) to inhibit SPP1 secretion in BMDMs (Fig. 5D, E). We found that supernatant of CVB3-stimulated BMDMs lead to increased *Ccl2* and *Ccl7* expression in cardiac fibroblasts, but that this effect was significantly diminished when SPP1 was inhibited (Fig. 5F). This finding suggested that BMDM-derived SPP1 could promote the transformation of fibroblasts to a *Ccl2*⁺*Ccl7*⁺ inflammatory phenotype in vitro. CCL2 and CCL7, also

known as monocyte chemoattractant protein-1 (MCP-1) and monocyte chemoattractant protein-3 (MCP-3), both belong to the CC chemokine family. Israel F. Charo et al. found defective recruitment of monocyte/macrophage to sites of inflammation in MCP-1 or MCP-3 knockout mice, suggesting that MCP-1 and MCP-3 were essential for monocyte/macrophage mobilization and recruitment of monocytes to inflamed tissues [18]. This suggests that inflammatory phenotypic transformation of fibroblasts may influence the course of VMC by regulating monocyte/macrophage migration.

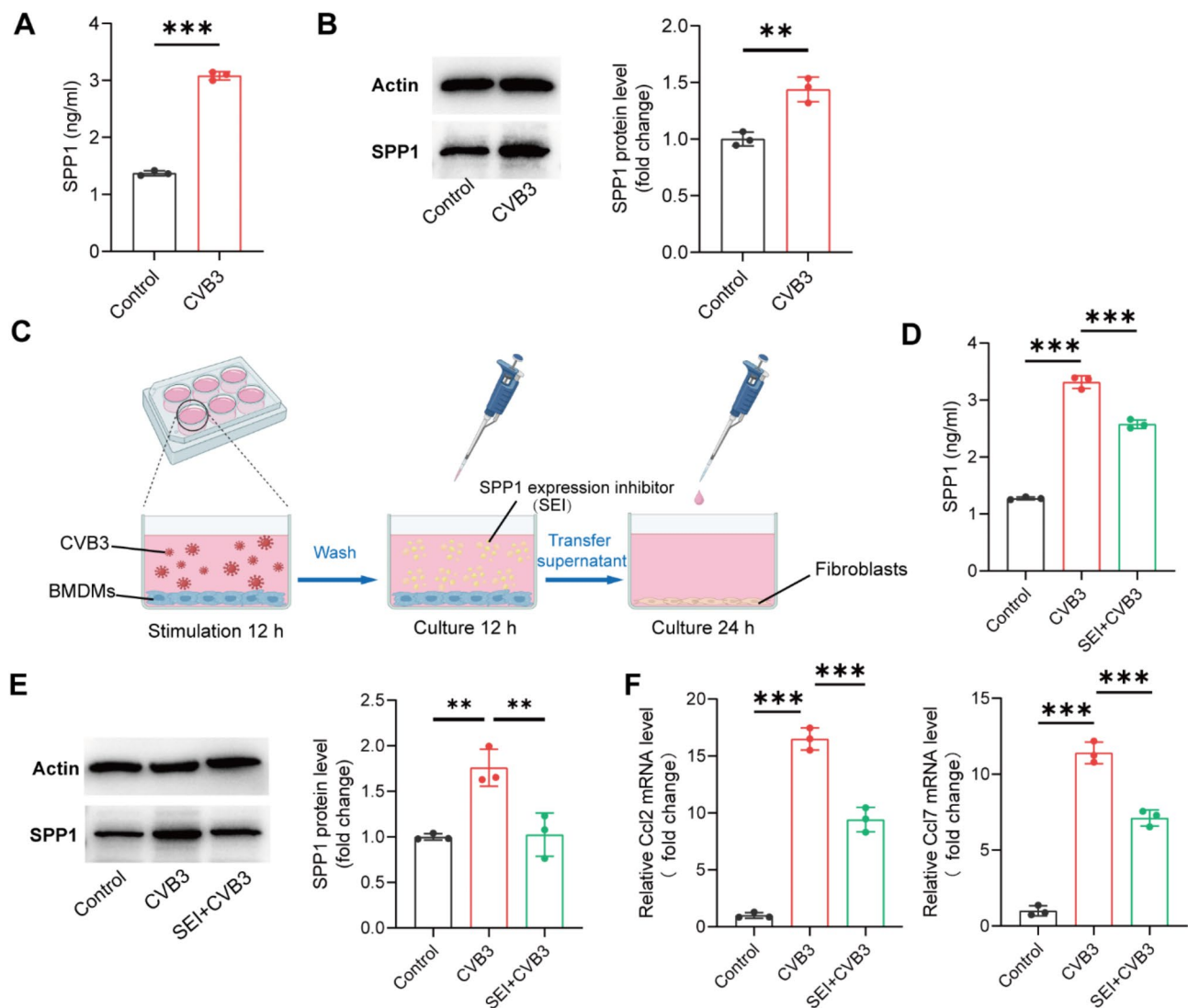


Fig. 5 Macrophage-derived SPP1 upregulates the expression of *Ccl2* and *Ccl7* in cardiac fibroblasts in vitro. **(A)** The expression levels of SPP1 in the supernatant of BMDMs with or without CVB3 stimulation. **(B)** Western blotting analysis of SPP1 in BMDMs with or without CVB3 stimulation. **(C)** Schematic diagram showing the process of co-culture of BMDMs and fibroblasts with CVB3 stimulation and SPP1 inhibition. **(D)** The expression levels of *Spp1* in the supernatant of BMDMs from control, CVB3 and SEI+CVB3 groups. **(E)** Western blotting analysis of SPP1 in BMDMs from control, CVB3 and SEI+CVB3 groups. **(F)** Relative *Ccl2* and *Ccl7* mRNA levels of cardiac fibroblasts from control, CVB3 and SEI+CVB3 groups. Unpaired t-test (two groups) and ANOVA (three groups) was used for analysis. Data are presented as mean \pm SD ($n=3$ biologically independent samples). *** $P < 0.001$, ** $P < 0.01$, * $P < 0.05$, ns $P > 0.05$

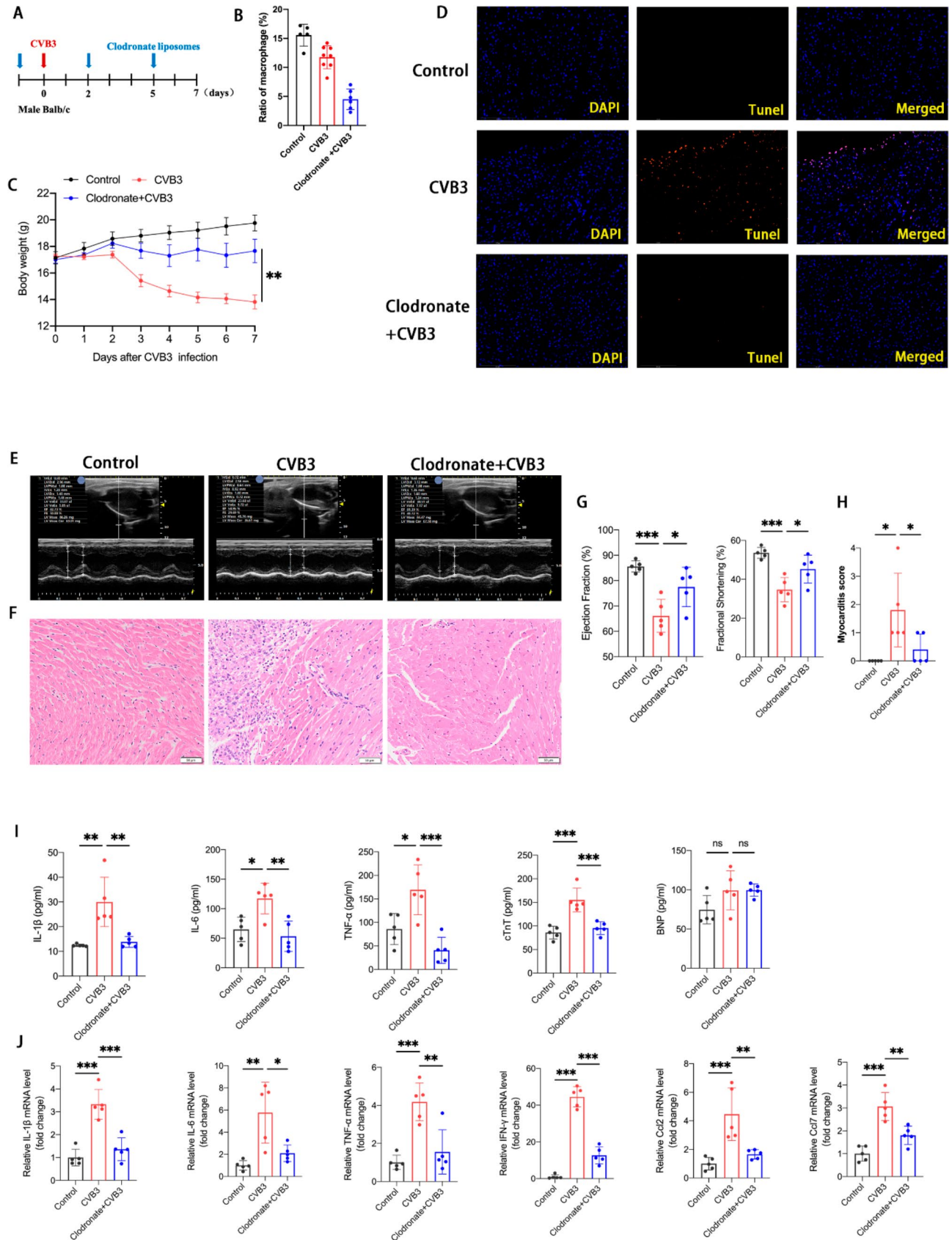


Fig. 6 (See legend on next page.)

(See figure on previous page.)

Fig. 6 Macrophage depletion at an early stage alleviates myocardial inflammation in VMC mice: **(A)** Timeline of macrophage depletion treatment. **(B)** Ratio of macrophages in spleen from control, CVB3 and Clodronate+CVB3 mice. **(C)** Weight changes of the three groups in the following 7 days after treatment. **(D)** Representative TUNEL staining of heart sections from control, CVB3 and Clodronate+CVB3 mice. **(E)** Representative parasternal long axis 2-dimensional and M-mode echocardiography images from control, CVB3 and Clodronate+CVB3 mice. **(F)** Cardiac immune infiltration status in different groups. Scale bars: 50 μ m. **(G)** EF and FS of control, CVB3 and Clodronate+CVB3 mice. **(H)** Myocarditis scores for cardiac immune infiltration from control, CVB3 and Clodronate+CVB3 mice. **(I)** The levels of inflammatory cytokines (IL-1 β , IL-6, TNF- α), cTnT and BNP in plasma from control, CVB3 and Clodronate+CVB3 mice. **(J)** Relative mRNA levels of inflammatory factors (IL-1 β , IL-6, TNF- α , IFN- γ), *Ccl2* and *Ccl7* of cardiac tissues from control, CVB3 and Clodronate+CVB3 mice. ANOVA was used for analysis. Data are presented as mean \pm SD ($n=5$ biologically independent samples). *** $P < 0.001$, ** $P < 0.01$, * $P < 0.05$, ns $P > 0.05$

To determine whether SPP1 has a direct effect on cardiomyocytes, we used the conditioned medium of BMDMs treated with CVB3 or SEI as described above to culture HL-1 cells. After 24 h, we detected apoptosis rates of HL-1 cells by flow cytometry, and there were not statistically different among the three groups (Figure S4A, B). Similarly, there was no significant change in cTnT levels in cell supernatants (Figure S4C). To further validate this result, we stimulated HL-1 cells with 100 ng/ml of SPP1 recombinant protein and there were also no differences in cell apoptosis or cTnT levels (Figure S4D~F). The CCK-8 cytotoxicity assay showed no direct toxic effect of SPP1 on HL-1 cells (Figure S4G). These results indicated that SPP1 might be involved in the progression of VMC through an immune response rather than directly damaging cardiomyocytes.

Macrophage depletion alleviates myocardial inflammation and reduces cardiac SPP1 levels in VMC mice

We next used clodronate liposomes to deplete macrophages in VMC mice to further investigate the role of macrophages during the acute phases of VMC (Fig. 6A). Macrophage reduction was confirmed using flow cytometry of spleen tissue, although macrophage levels were not completely depleted in our model (Fig. 6B). Early use of clodronate liposomes significantly ameliorated CVB3 infection-induced weight loss (Fig. 6C) and reduced cellular apoptosis in cardiomyocytes as measured by TUNEL (Fig. 6D). Echocardiography showed significantly enhanced cardiac function, with increased EF and FS (Fig. 6E, G). Cardiac immune cell infiltration was also markedly reduced (Fig. 6F, H). We found decreased expression of inflammatory factors (IL-1 β , IL-6, TNF- α) and cTnT in plasma, but BNP levels remained unchanged (Fig. 6I). We also found decreased expression of inflammatory factors (IL-1 β , IL-6, TNF- α , IFN- γ) in the heart as well as decreased chemokines *Ccl2* and *Ccl7* (Fig. 6J). These findings suggested that inflammation was suppressed in mice with VMC after the inhibition or removal of macrophages. Collectively, these results suggested that partial depletion of macrophages alleviated acute inflammation and improved cardiac function in VMC mice. This indicated that immune damage caused by excessive macrophage recruitment and infiltration is detrimental to the heart during the acute VMC phase.

To investigate *Spp1* expression levels, as well as their relationship with macrophages in VMC, we measured *Spp1* mRNA and protein levels in the plasma and hearts of both VMC mice and macrophage depletion mice. *Spp1* expression levels were significantly increased in the VMC group, and *Spp1* was significantly reduced in both hearts and plasma after macrophage depletion (Fig. 7A~D). Immunofluorescence suggested co-localization of macrophages and SPP1 in the heart, and verified increased SPP1 in macrophages in the VMC mice and synchronized reduction after macrophage depletion (Fig. 7E). These data indicated that increases in SPP1 during VMC were mainly driven by macrophages.

Inhibition of SPP1 alleviates acute myocardial inflammation and improves cardiac function in VMC mice

Because SPP1 level was significantly increased in our VMC model, we explored whether SPP1 inhibitors would have therapeutic effects in VMC. SEI was injected one day before CVB3 infection, with additional injections given every other day for a total of three injections (Fig. 8A). Western blots and ELISA showed that SPP1 expression decreased significantly in both cardiac tissue and plasma (Fig. 8C, D). Treatment with SEI did not ameliorate weight loss in infected mice (Fig. 8B). However, SEI did significantly decrease *Ccl2* and *Ccl7* expression (Fig. 8E) and macrophage infiltration in VMC mice (Fig. 8F). Because both macrophages and fibroblasts can produce *Ccl2* and *Ccl7*, we could not verify causality in these changes. And it was clear that SPP1 inhibition reduced cardiac macrophage infiltration. Echocardiography revealed significantly enhanced cardiac function, with increases in EF and FS, in the SEI group (Fig. 8G, I). Cardiac immune cell infiltration (Fig. 8H, J) and cellular apoptosis (Fig. 8K) were markedly reduced. There were also simultaneous reduction in inflammatory factors (IL-1 β , IL-6, TNF- α , IFN- γ) and cTnT in mice plasma and cardiac tissue (Fig. 8L, M and Figure S5). These findings were similar to those determined with the previously performed macrophage depletion. We also showed that cardiac *Spp1* mRNA expression was decreased following SEI treatment (Fig. 8N), which may be due to reductions in macrophage levels.

In summary, inhibition of SPP1 successfully decreased the severity of inflammation and immune infiltration in

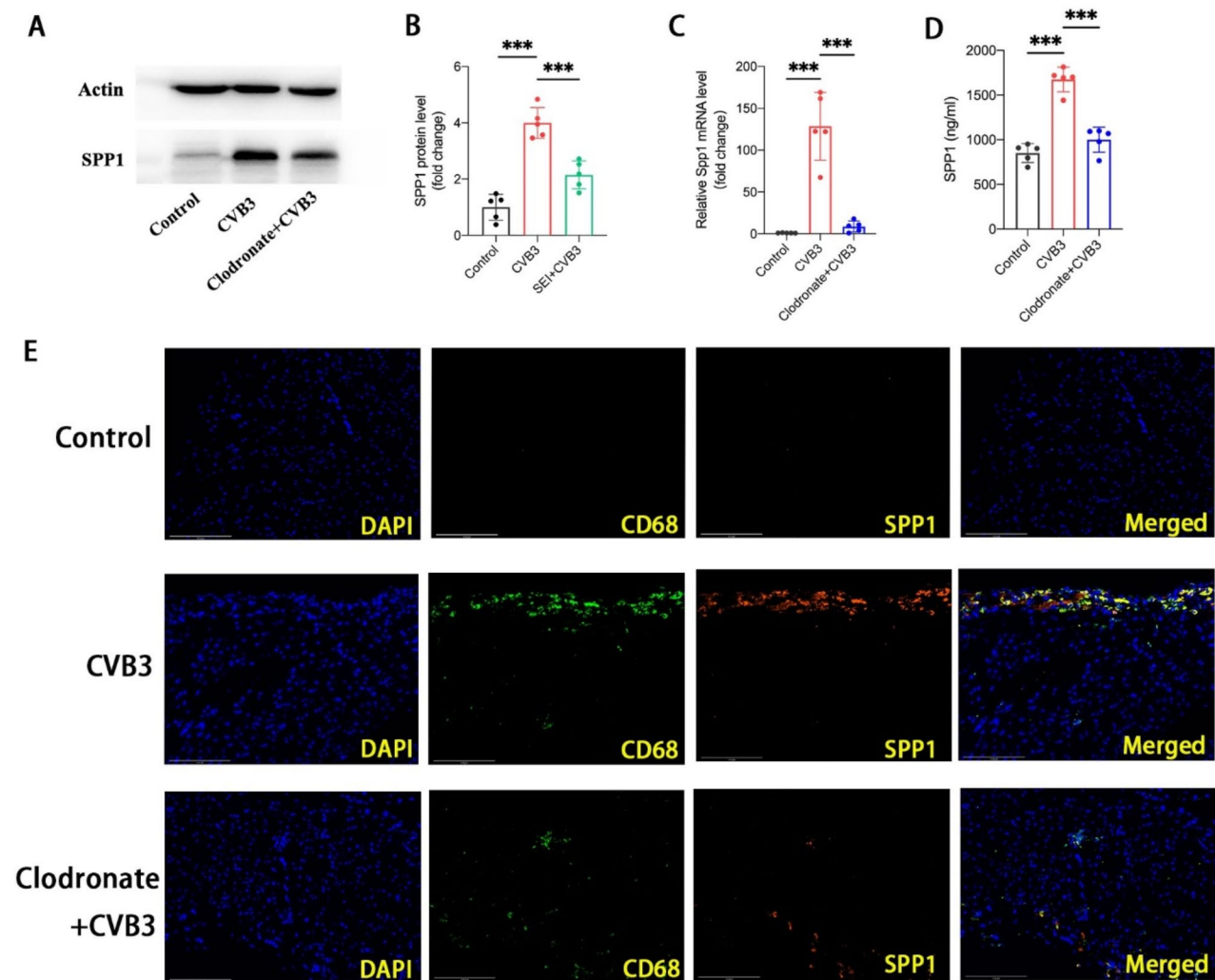


Fig. 7 Macrophage depletion reduces SPP1 levels in VMC mice: **(A)** The Western blot results of SPP1 protein expression in cardiac tissues from control, CVB3 and Clodronate + CVB3 mice. **(B)** The quantitative analysis for Western blot results of SPP1 protein expression in the cardiac tissues. **(C)** Relative *Spp1* mRNA levels of cardiac tissues from control, CVB3 and Clodronate + CVB3 mice. **(D)** The expression levels of SPP1 in plasma from control, CVB3 and Clodronate + CVB3 mice. **(E)** Representative immunofluorescent staining of macrophages (CD68, green), nuclei (DAPI, blue) and SPP1 (red) in cardiac tissues from control, CVB3 and Clodronate + CVB3 mice. Scale bars: 125 μ m. ANOVA was used for analysis. Data are presented as mean \pm SD ($n=5$ biologically independent samples). *** $P < 0.001$, ** $P < 0.01$, * $P < 0.05$, ns $P > 0.05$

the heart, and improved cardiac function, in VMC mice. We also examined plasma SPP1 levels in both healthy and acute myocarditis patients. SPP1 levels showed more than 2-fold elevation in the myocarditis group (Fig. 8O). Our findings highlight the clinical value of SPP1 as a biomarker for myocarditis.

Discussion

Research on the immune mechanisms underlying myocarditis has increased over the past several years, but the pathophysiological mechanisms remain elusive. Here, we used an established viral myocarditis (VMC) model to construct a time series and better understand the immunologic changes in the condition [23, 24]. Our mouse model suggested that day 7 after CVB3 infection was

the peak inflammatory period, which was largely consistent with previous studies [25, 26]. We also depicted the single-cell landscape of cardiac tissue during the acute phase of VMC, and found that macrophage populations expanded more than any other immune cell type, while fibroblast populations were significantly reduced. We additionally demonstrated a population of *Spp1*⁺ macrophages which had deleterious effects in VMC. Interestingly, this macrophage population may self-recruit by stimulating fibroblasts to shift toward a *Ccl2*⁺*Ccl7*⁺ inflammatory phenotype, leading to more severe immune injuries in the heart.

We first observed impaired cardiac function in mice on day 4 after CVB3 infection, which was followed by the infiltration of a large number of immune cells and further

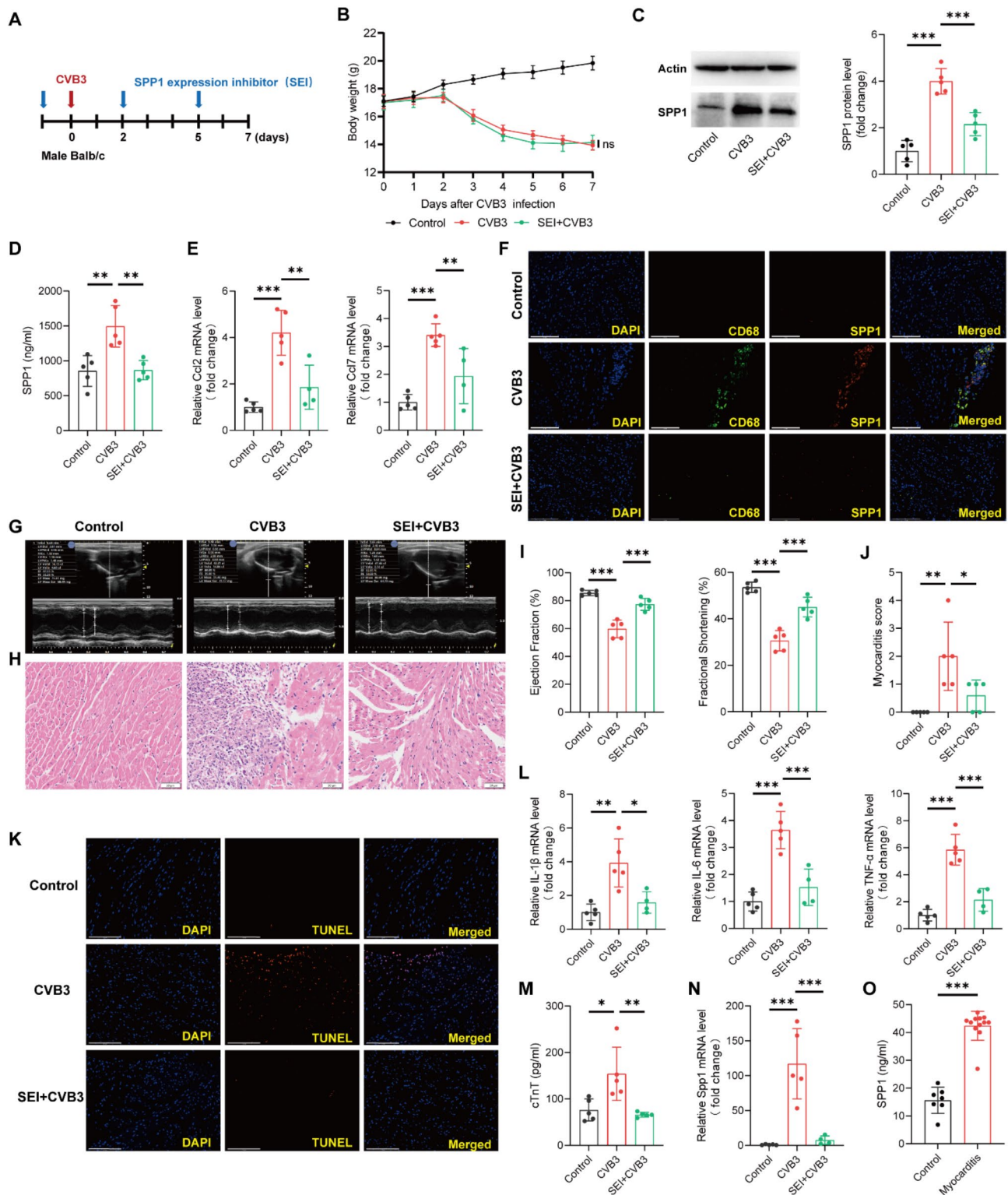


Fig. 8 (See legend on next page.)

cardiac dysfunction. This is consistent with a previous study by Daowen Wang et al. [6]. Our findings suggest that macrophages are the major immune cells which infiltrate the heart and drive inflammation during the acute

phase of VMC [23, 27]. During the initial phases VMC, cardiotropic viruses enter the heart and cause direct tissue damage [28]. However, secondary immune-mediated damage often exceeds viral pathogenicity [29]. On the

(See figure on previous page.)

Fig. 8 Inhibition of SPP1 alleviates myocardial injury in VMC mice: **(A)** Timeline of SPP1 inhibition treatment. **(B)** Weight changes of the control, CVB3 and SEI+CVB3 mice in the following 7 days after treatment. **(C)** Western blotting analysis of SPP1 in cardiac tissues from control, CVB3 and SEI+CVB3 mice. **(D)** The expression levels of SPP1 in plasma from control, CVB3 and SEI+CVB3 mice. **(E)** Relative *Ccl2* and *Ccl7* mRNA levels of cardiac tissues from control, CVB3 and SEI+CVB3 mice. **(F)** Representative immunofluorescent staining of macrophages (CD68, green), nuclei (DAPI, blue) and SPP1 (red) in cardiac tissues from control, CVB3 and SEI+CVB3 mice. Scale bars: 125 μm . **(G)** Representative parasternal long axis 2-dimensional and M-mode echocardiography images from control, CVB3 and SEI+CVB3 mice. **(H)** Cardiac immune infiltration status in different groups. Scale bars: 50 μm . **(I)** EF and FS of control, CVB3 and SEI+CVB3 mice. **(J)** Myocarditis scores for cardiac immune infiltration from control, CVB3 and SEI+CVB3 mice. **(K)** Representative TUNEL staining of heart sections from control, CVB3 and SEI+CVB3 mice. **(L)** Relative mRNA levels of inflammatory factors (IL-1 β , IL-6, TNF- α) in cardiac tissues from control, CVB3 and SEI+CVB3 mice. **(M)** The levels of cTnT in mouse plasma. **(N)** Relative *Spp1* mRNA levels of cardiac tissues from control, CVB3 and SEI+CVB3 mice. **(O)** The levels of SPP1 in plasma from control and myocarditis children. ANOVA was used for analysis. Data are presented as mean \pm SD ($n \geq 5$ biologically independent samples). *** $P < 0.001$, ** $P < 0.01$, * $P < 0.05$, ns $P > 0.05$

seventh day following CVB3 infection, we found that macrophage phagocytosis, lysis, cellular senescence, and metabolic activity were all markedly increased, indicating that macrophages were extensively eliminating both infected and uninfected cells. When immune responses are not terminated in a timely fashion, indiscriminate macrophage activity can lead to further myocardial damage. These indiscriminate macrophage attacks may be a major cause of fibroblast reduction. Macrophages play an important role in myocarditis pathogenesis. The development of single-cell transcriptomics has allowed for more detailed study of macrophage populations and diversity. Kory J Lavine et al. reported on a population of *Cxcl9*⁺*Cxcl10*⁺ macrophages in ICI myocarditis, and found that blockade of IFN- γ could be a powerful therapeutic option [5]. Xiangming Fang et al. found a protective role for TREM2^{hi} resident macrophages in Sepsis-induced cardiomyopathy [30]. These studies demonstrated the heterogeneity of different macrophage populations in differing myocardial inflammatory diseases. Our study identified a myocarditis-specific macrophage subpopulation characterized by high *Spp1* expression. This population of macrophages is derived from peripheral blood mononuclear cells, and undergo an almost *de novo* expansion in VMC. These macrophages had the highest acute inflammatory scores among all of the macrophage clusters we identified, despite the fact that the transcriptomic profiles most closely matched M2 macrophage phenotypes. Previous studies have shown that *Spp1* plays an inflammatory chemotactic role in a variety of cardiovascular system diseases [31–33]. This suggests that relying solely on the traditional M1/M2 classification system can limit the study of macrophage function and heterogeneity. In many cases, macrophages cannot be identified by binary classification schemes [34, 35]. Our study provides a reference for macrophage classification in the acute phase of VMC in mice.

We next analyzed fibroblast population changes in VMC. We found that the chemokines *Ccl2* and *Ccl7* were upregulated, and that these upregulations were related to increased monocyte chemotaxis. Phenotypic fibroblast shifts can emphasize the differing immune functions performed by certain subpopulations [36]. Our sequencing

data suggested that *Spp1*⁺ macrophages enhanced interactions with inflammatory fibroblasts via the integrin complex. In vitro stimulation of cardiac fibroblasts with BMDM-derived SPP1 increased *Ccl2* and *Ccl7* expression, but the exact mechanism underlying these changes requires further investigation. Nevertheless, the therapeutic role of CCL2 inhibition in VMC has been demonstrated. Previous studies have shown that specific antibody blockade of CCL2 reduced monocyte migration in mice with VMC and attenuated myocardial inflammation [37]. We also found that CVB3 could directly stimulate macrophages to secrete SPP1 without being mediated by other cytokines. This finding suggests that viral exposure can directly lead to macrophage activation, and act as a trigger for severe inflammatory responses.

SPP1 levels were significantly elevated in the cardiac tissue and peripheral blood of mice with VMC. We found that SPP1 expression levels plummeted after macrophage depletion, suggesting that macrophages are the major source of SPP1 in VMC mice. Further studies demonstrated that early inhibition or removal of macrophages improved the overall health conditions of mice with VMC, including increased body weight, better cardiac functioning, and more well-regulated cardiomyocyte apoptosis, as well as reduced cytokine release. Interestingly, previous studies have shown that complete macrophage depletion contributes to increased viral replication and mortality in mice, but is also related to decreases in the severity of acute myocarditis and chronic fibrosis [38]. Our study emphasizes that macrophages dominate both the proinflammatory and deleterious effects in acute VMC. Understanding how to best mitigate the proinflammatory role of macrophages at an appropriate time should be a major focus of future research in VMC.

Finally, we showed that inhibiting SPP1 was sufficient to reduce cardiac injury, cardiac inflammation, and macrophage accumulation in the heart. Downregulation of *Ccl2/Ccl7* was also detected in cardiac tissue. However, in vivo environments are also complex and variable. Based on previous reports, these downregulations may result from more than just decreases in fibroblast secretion. For example, CCL2 is produced by a variety of cells following myocardial injuries [39], but SPP1 also

promotes macrophage secretion of CCL2 [40]. Macrophage recruitment in the heart is clearly inhibited by *Ccl2/Ccl7* downregulation when SPP1 levels are reduced. Our study provides a preliminary indication that SPP1 can influence the inflammatory infiltrate in the heart by regulating the expression of *Ccl2/Ccl7* in fibroblasts. Cardiomyocytes cultured in vitro were not directly affected by SPP1, emphasizing the role of SPP1 as an inflammatory cytokine in VMC. Our findings imply that macrophage-released SPP1 amplifies immune cascades and leads to sustained immune responses. This provides new insight into the pathogenesis of VMC. In addition, research has shown that SPP1 is associated with fibrosis in VMC [41], and we found elevated plasma SPP1 levels in patients with acute myocarditis, suggesting that SPP1 may be a marker of persistent inflammation.

Our study has some limitations. Because of restrictions inherent to the 10x Genomics Chromium platform, we lack transcriptomic information about cardiomyocytes, which limits a complete understanding of myocardial injury. Besides, our study demonstrates that the partial depletion of macrophages during the acute phase in VMC attenuates myocarditis, but the degree of this suppression remains unknown. Macrophages are involved in both viral clearance and immune response regulation. Considering the positive role of macrophages in immune responses, over-depletion of macrophages may not lead to benefits, and inhibiting SPP1 production may be a better therapeutic alternative. Another important aspect is that we did not investigate whether CVB3-induced myocarditis is attenuated in mice with macrophage-deficient *Spp1*. We have confirmed the attenuation of the myocardial inflammation in mice after using SPP1 expression inhibitor. In the following study, we will further investigate the role of macrophage-derived SPP1 in myocarditis using mice with macrophage-specific deletion of *Spp1*. Thus, SPP1's mechanism of action in VMC needs future study in order to provide novel insights about potential future therapies.

Our study provides the first evidence of crosstalk between inflammatory fibroblasts and macrophages during the acute phase of VMC. It also demonstrates the proinflammatory role of SPP1, providing important insights into the immunopathogenesis of VMC. Our study highlights that disrupting the positive feedback loop of macrophage self-recruitment by inhibiting SPP1 may be a promising therapeutic strategy for VMC. The use of elevations in plasma SPP1 levels as a marker for inflammation will also help us selectively administer therapies.

Abbreviations

VMC	Viral myocarditis
CVB	Coxsackie virus B
EAM	Experimental autoimmune myocarditis

ICI	Immune checkpoint inhibitor
PBS	Phosphate buffer solution
SPP1	Secreted Phosphoprotein 1
BMDM	Bone marrow-derived macrophage
SEI	SPP1 expression inhibitor
DMSO	Dimethyl sulfoxide
HE	Hematoxylin-eosin
EF	Ejection fraction
FS	Fractional shortening
RT-qPCR	Real-time quantitative PCR
ELISA	Enzyme-linked immunosorbent assay
BNP	B-type natriuretic peptide
cTnT	Cardiac troponin T
scRNA-seq	Single-cell RNA sequencing
UMAP	Uniform Manifold Approximation and Projection
SNN	Shared nearest neighbor
log2FC	Log2 Fold Change
DEG	Define differentially expressed gene
KEGG	Kyoto Encyclopedia of Genes and Genomes
GO	Gene Ontology
ANOVA	One-way analysis of variance
NK	Natural killer
DC	Dendritic
MHC	Major histocompatibility complex
MCP-1	Monocyte chemoattractant protein-1
MCP-3	Monocyte chemoattractant protein-3

Supplementary Information

The online version contains supplementary material available at <https://doi.org/10.1186/s13062-025-00621-2>.

Supplementary Material 1

Supplementary Material 2

Acknowledgements

We thank the staff of LC-Bio Technology Co. Ltd (Hangzhou, China) for offering technical support. We would like to express the Institute of Pathogenic Biology, Clinical and Basic Medical School, Shandong First Medical University for providing CVB3. Figure 2 A and Fig. 5 C were created with BioRender.com.

Author contributions

BH and LZ designed this study. KYL and KYG were responsible for the sample collection. XYD carried out the data analysis. XYD, KYL, YNY carried out the experiments. SZ operated the Echocardiography. HLJ provided the administrative support. XYD and LZ wrote the original manuscript. All authors read and approved the final manuscript.

Funding

This study was supported by the Taishan Scholar Foundation of Shandong Province (no. 201511099), the Jinan Science and Technology Bureau (after subsidy) (no. 202134015), the Natural Science Foundation of Shandong Provincial (ZR2023QH296), the Natural Science Foundation of Shandong Provincial (ZR2023MH052) and the Shandong Provincial Clinical Research Center for Children's Health and Disease office.

Data availability

No datasets were generated or analysed during the current study.

Declarations

Ethical approval

The study was carried out in compliance with the Helsinki Declaration and was authorized by the Institutional Ethics Committee of Shandong Provincial Hospital. Informed consents were obtained from all donors or their guardians. The animal study was approved by the Institutional Animal Research Committee of Shandong Provincial Hospital.

Competing interests

The authors declare no competing interests.

Author details

¹Department of Pediatric Cardiology, Cheeloo College of Medicine, Shandong Provincial Hospital, Shandong University, Jinan, Shandong, China

²Department of Pediatric Cardiology, Shandong Provincial Hospital Affiliated to Shandong First Medical University, Jinan, Shandong, China

³Shandong Provincial Clinical Research Center for Children's Health and Disease office, Shandong Provincial Hospital, Jinan, Shandong, China

⁴Shandong First Medical University & Shandong Academy of Medical Sciences, Jinan, Shandong, China

⁵Medical Science and Technology Innovation Center, Shandong First Medical University, Shandong Academy of Medical Sciences, Jinan, Shandong, China

⁶Rui Jin Hospital Nanxiang Branch, Shanghai 201802, China

Received: 9 January 2025 / Accepted: 22 February 2025

Published online: 14 March 2025

References

- Law YM, Lal AK, Chen S, Cihakova D, Cooper LT Jr, Deshpande S, Godown J, Grosse-Wortmann L, Robinson JD, Towbin JA, et al. Diagnosis and management of myocarditis in children: A scientific statement from the American heart association. *Circulation*. 2021;144(6):e123–35.
- Heymans S, Eriksson U, Lehtonen J, Cooper LT Jr. The quest for new approaches in myocarditis and inflammatory cardiomyopathy. *J Am Coll Cardiol*. 2016;68(21):2348–64.
- Caforio AL, Pankuweit S, Arbustini E, Basso C, Gimeno-Blanes J, Felix SB, Fu M, Helio T, Heymans S, Jahns R, et al. Current state of knowledge on aetiology, diagnosis, management, and therapy of myocarditis: a position statement of the European society of cardiology working group on myocardial and pericardial diseases. *Eur Heart J*. 2013;34(33):2636–48. 2648a–2648d.
- Hua X, Hu G, Hu Q, Chang Y, Hu Y, Gao L, Chen X, Yang PC, Zhang Y, Li M, et al. Single-Cell RNA sequencing to dissect the immunological network of autoimmune myocarditis. *Circulation*. 2020;142(4):384–400.
- Ma P, Liu J, Qin J, Lai L, Heo GS, Luehmann H, Sultan D, Bredemeyer A, Bajapa G, Feng G, et al. Expansion of pathogenic cardiac macrophages in immune checkpoint inhibitor myocarditis. *Circulation*. 2024;149(1):48–66.
- Li H, Zhang M, Zhao Q, Zhao W, Zhuang Y, Wang J, Hang W, Wen Z, Wang L, Chen C, et al. Self-recruited neutrophils trigger over-activated innate immune response and phenotypic change of cardiomyocytes in fulminant viral myocarditis. *Cell Discov*. 2023;9(1):103.
- Litvinukova M, Talavera-Lopez C, Maatz H, Reichart D, Worth CL, Lindberg EL, Kanda M, Polanski K, Heinig M, Lee M, et al. Cells of the adult human heart. *Nature*. 2020;588(7838):466–72.
- Wu L, Ong S, Talor MV, Barin JG, Baldeviano GC, Kass DA, Bedja D, Zhang H, Sheikh A, Margolick JB, et al. Cardiac fibroblasts mediate IL-17A-driven inflammatory dilated cardiomyopathy. *J Exp Med*. 2014;211(7):1449–64.
- Grabie N, Delfs MW, Westrich JR, Love VA, Stavrakis G, Ahmad F, Seidman CE, Seidman JG, Lichtman AH. IL-12 is required for differentiation of pathogenic CD8+T cell effectors that cause myocarditis. *J Clin Invest*. 2003;111(5):671–80.
- Stuart T, Butler A, Hoffman P, Hafemeister C, Papalexi E, Mauck WM 3rd, Hao Y, Stoerckius M, Smitert P, Satija R. Comprehensive integration of Single-Cell data. *Cell*. 2019;177(7):1888–902. e1821.
- Huber S, Shi C, Budd RC. Gammadelta T cells promote a Th1 response during coxsackievirus B3 infection in vivo: role of Fas and Fas ligand. *J Virol*. 2002;76(13):6487–94.
- Nishio R, Matsumori A, Shioi T, Ishida H, Sasayama S. Treatment of experimental viral myocarditis with interleukin-10. *Circulation*. 1999;100(10):1102–8.
- Wei B, Deng Y, Huang Y, Gao X, Wu W. IL-10-producing B cells attenuate cardiac inflammation by regulating Th1 and Th17 cells in acute viral myocarditis induced by Coxsackie virus B3. *Life Sci*. 2019;235:116838.
- Hou X, Chen G, Bracamonte-Baran W, Choi HS, Diny NL, Sung J, Hughes D, Won T, Wood MK, Talor MV, et al. The cardiac microenvironment instructs divergent monocyte fates and functions in myocarditis. *Cell Rep*. 2019;28(1):172–e189177.
- Papritz K, Savvatis K, Koschel A, Miteva K, Tschöpe C, Van Linthout S. Cardiac (myo)fibroblasts modulate the migration of monocyte subsets. *Sci Rep*. 2018;8(1):5575.
- Chen R, Zhang H, Tang B, Luo Y, Yang Y, Zhong X, Chen S, Xu X, Huang S, Liu C. Macrophages in cardiovascular diseases: molecular mechanisms and therapeutic targets. *Signal Transduct Target Ther*. 2024;9(1):130.
- Icer MA, Gezmen-Karadag M. The multiple functions and mechanisms of osteopontin. *Clin Biochem*. 2018;59:17–24.
- Tsou CL, Peters W, Si Y, Slaymaker S, Aslanian AM, Weisberg SP, Mack M, Charo IF. Critical roles for CCR2 and MCP-3 in monocyte mobilization from bone marrow and recruitment to inflammatory sites. *J Clin Invest*. 2007;117(4):902–9.
- Zhang YJ, Rutledge BJ, Rollins BJ. Structure/activity analysis of human monocyte chemoattractant protein-1 (MCP-1) by mutagenesis. Identification of a mutated protein that inhibits MCP-1-mediated monocyte chemotaxis. *J Biol Chem*. 1994;269(22):15918–24.
- Xuan Y, Chen C, Wen Z, Wang DW. The roles of cardiac fibroblasts and endothelial cells in myocarditis. *Front Cardiovasc Med*. 2022;9:882027.
- Forte E, Skelly DA, Chen M, Daigle S, Morelli KA, Hon O, Philip VM, Costa MW, Rosenthal NA, Furtado MB. Dynamic interstitial cell response during myocardial infarction predicts resilience to rupture in genetically diverse mice. *Cell Rep*. 2020;30(9):3149–e31633146.
- Patrick R, Janbandhu V, Tallapragada V, Tan SSM, McKinna EE, Contreras O, Ghazanfar S, Humphreys DT, Murray NJ, Tran YTH, et al. Integration mapping of cardiac fibroblast single-cell transcriptomes elucidates cellular principles of fibrosis in diverse pathologies. *Sci Adv*. 2024;10(25):eadk8501.
- Li K, Xu W, Guo Q, Jiang Z, Wang P, Yue Y, Xiong S. Differential macrophage polarization in male and female BALB/c mice infected with coxsackievirus B3 defines susceptibility to viral myocarditis. *Circ Res*. 2009;105(4):353–64.
- Huang Y, Huang X, Wei Z, Dong J, Lu J, Tang Q, Lu F, Cen Z, Wu W. CD4(+) T(EM) cells drive the progression from acute myocarditis to dilated cardiomyopathy in CVB3-induced BALB/c mice. *Int Immunopharmacol*. 2024;127:11304.
- Wu Y, Yue Y, Xiong S. Cardiac miR-19a/19b was induced and hijacked by CVB3 to facilitate virus replication via targeting viral genomic RdRp-encoding region. *Antiviral Res*. 2023;217:105702.
- Yue-Chun L, Gu XH, Li-Sha G, Zhou DP, Xing C, Guo XL, Pan LL, Song SY, Yu LL, Chen GY, et al. Vagus nerve plays a pivotal role in CD4+T cell differentiation during CVB3-induced murine acute myocarditis. *Virulence*. 2021;12(1):360–76.
- Leuschner F, Courties G, Dutta P, Mortensen LJ, Gorbatorov R, Sena B, Novobrantseva TI, Borodovsky A, Fitzgerald K, Koteliensky V, et al. Silencing of CCR2 in myocarditis. *Eur Heart J*. 2015;36(23):1478–88.
- Sagar S, Liu PP, Cooper LT. Jr. myocarditis. *Lancet*. 2012;379(9817):738–47.
- Liu PP, Mason JW. Advances in the Understanding of myocarditis. *Circulation*. 2001;104(9):1076–82.
- Zhang K, Wang Y, Chen S, Mao J, Jin Y, Ye H, Zhang Y, Liu X, Gong C, Cheng X, et al. TREM2(hi) resident macrophages protect the septic heart by maintaining cardiomyocyte homeostasis. *Nat Metab*. 2023;5(1):129–46.
- Ashkar S, Weber GF, Panoutsakopoulou V, Sanchirico ME, Jansson M, Zawaideh S, Rittling SR, Denhardt DT, Glimcher MJ, Cantor H. Eta-1 (osteopontin): an early component of type-1 (cell-mediated) immunity. *Science*. 2000;287(5454):860–4.
- Renault MA, Robbesyn F, Reant P, Douin V, Daret D, Allieres C, Belloc I, Couffignal T, Arnal JF, Klingel K, et al. Osteopontin expression in cardiomyocytes induces dilated cardiomyopathy. *Circ Heart Fail*. 2010;3(3):431–9.
- Wagenhauser MU, Mulorz J, Krott KJ, Bosbach A, Feige T, Rhee YH, Chatterjee M, Petzold N, Boddeker C, Ibing W, et al. Crosstalk of platelets with macrophages and fibroblasts aggravates inflammation, aortic wall stiffening, and osteopontin release in abdominal aortic aneurysm. *Cardiovasc Res*. 2024;120(4):417–32.
- Stables MJ, Shah S, Camon EB, Lovering RC, Newson J, Bystrom J, Farrow S, Gilroy DW. Transcriptomic analyses of murine resolution-phase macrophages. *Blood*. 2011;118(26):e192–208.
- Stoger JL, Gijbels MJ, van der Velden S, Manca M, van der Loos CM, Biessen EA, Daemen MJ, Lutgens E, de Winther MP. Distribution of macrophage polarization markers in human atherosclerosis. *Atherosclerosis*. 2012;225(2):461–8.
- Cavagnero KJ, Gallo RL. Essential immune functions of fibroblasts in innate host defense. *Front Immunol*. 2022;13:1058862.
- Shen Y, Xu W, Chu YW, Wang Y, Liu QS, Xiong SD. Coxsackievirus group B type 3 infection upregulates expression of monocyte chemoattractant protein 1 in cardiac myocytes, which leads to enhanced migration of mononuclear cells in viral myocarditis. *J Virol*. 2004;78(22):12548–56.

38. De Jaquenod C, Ure AE, Rivadeneyra L, Schattner M, Gomez RM. Macrophages and galectin 3 play critical roles in CVB3-induced murine acute myocarditis and chronic fibrosis. *J Mol Cell Cardiol.* 2015;85:58–70.
39. Deshmane SL, Kremlev S, Amini S, Sawaya BE. Monocyte chemoattractant protein-1 (MCP-1): an overview. *J Interferon Cytokine Res.* 2009;29(6):313–26.
40. Rowe GC, Raghuram S, Jang C, Nagy JA, Patten IS, Goyal A, Chan MC, Liu LX, Jiang A, Spokes KC, et al. PGC-1alpha induces SPP1 to activate macrophages and orchestrate functional angiogenesis in skeletal muscle. *Circ Res.* 2014;115(5):504–17.
41. Szalay G, Sauter M, Haberland M, Zuegel U, Steinmeyer A, Kandolf R, Klingel K. Osteopontin: a fibrosis-related marker molecule in cardiac remodeling of enterovirus myocarditis in the susceptible host. *Circ Res.* 2009;104(7):851–9.

Publisher's note

Springer Nature remains neutral with regard to jurisdictional claims in published maps and institutional affiliations.